The Effect of I/Q Imbalance and Complex Filter Component Mismatch in Low-IF Receivers

Jirayuth Mahattanakul, *Member, IEEE*

***Abstract*—In this paper, the effect of mismatch in the front-end section of the low intermediate-frequency (IF) receiver is investigated. In particular, the I/Q imbalance in quadrature mixing and component mismatch in complex filtering are concurrently taken into consideration. It is shown that the signal to interference ratio of the low-IF receiver cannot be generally improved by increasing the order of complex filter.**

***Index Terms*—CMOS analog integrated circuits, complex filters, low-intermediate-frequency (IF) receivers, quadrature mixer.**

I. Introduction

THANKS to its insensitivity to dc offset and a high degree of integration, low-intermediate-frequency (IF) receiver [1], [2], which combines the advantages of both IF and zero-IF receivers, has received much attention recently. The topology of the low-IF receiver, shown in Fig. 1, is closely related to that of the zero-IF receiver. The principle of the low-IF receiver is based upon the use of quadrature mixing and complex or polyphase filtering.

In practice, the limitation of low-IF receiver is due to imperfect matching in analog integrated implementation. For quadrature downconversion, the effect of I/Q imbalance results in the leakage of the image signal into the wanted channel [2]–[4], reducing the signal to interference ratio. Component mismatch in complex filter implementation also contributes the crosstalk between the wanted channel and the image channel [5], [6]. In this paper, we will study the combined effect of complex filter mismatch and I/Q imbalance in the low-IF receiver.

It should be noted that apart from Fig. 1, there are other variations of the low-IF receiver including the topology using real IF filters [2], [4] and the topology using the polyphase filter as an RF I/Q generator [7]. The selection of topology has to be done using on various criteria, e.g., sensitivity, robustness, power consumption and level of integration [8]. The topology selection, however, is beyond the scope of this work, which is primary concerned with the low-IF topology shown in Fig. 1.

II. Mismatch in Low-IF Receiver

Ideally, quadrature frequency conversion in zero-IF and low-IF receiver is done by multiplying RF signal with two sinusoidal signals with equal amplitude and 90° phase difference. However in practice, as shown in Fig. 1, there are always imbalance in both amplitude and phase between the two quadrature signals.

Manuscript received January 18, 2005; revised May 9, 2005, and August 3, 2005. This paper was recommended by Associate Editor I. M. Filanovsky.

The author is with the Mahanakorn University of Technology, Bangkok 10530, Thailand (e-mail: jirayut@mut.ac.th).

Digital Object Identifier 10.1109/TCSI.2005.857545

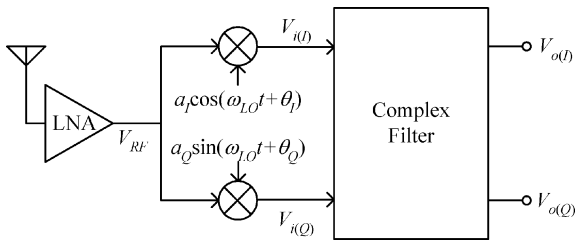

Fig. 1. Front-end topology of a low-IF receiver.

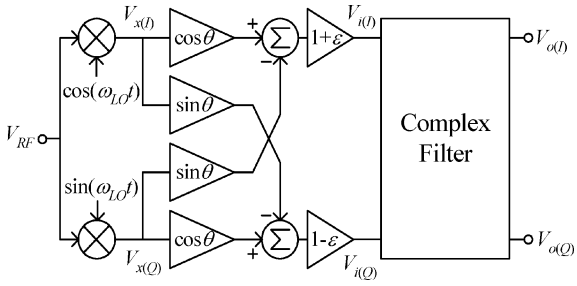

Fig. 2. Block diagram representation of Fig. 1.

According to Fig. 1, by denoting

$$a_O = \frac{(a_I + a_Q)}{2} \quad \text{and} \quad \Delta a = a_I - a_Q$$
$$\text{and } \theta_O = \frac{(\theta_I + \theta_Q)}{2} \quad \text{and} \quad \Delta\theta = \theta_I - \theta_Q$$

we found that

$$v_{iI(I)}(t) = v_{\mathrm{RF}}(t) a_o (1+\varepsilon)\cos(\omega_{\mathrm{LO}} t + \theta_o + \theta) \quad (1)$$
$$v_{iI(Q)}(t) = v_{\mathrm{RF}}(t) a_o (1-\varepsilon)\sin(\omega_{\mathrm{LO}} t + \theta_o - \theta) \quad (2)$$

where $\varepsilon = 0.5(\Delta a/a_O)$ and $\theta = 0.5\Delta\theta$.

Thus in a normalized case, i.e., $a_O = 1$ and $\theta_O = 0$, by defining

$$v_{x(I)}(t) = v_{\mathrm{RF}}(t)\cos(\omega_{\mathrm{LO}} t) \quad (3)$$

and

$$v_{x(Q)}(t) = v_{\mathrm{RF}}(t)\sin(\omega_{\mathrm{LO}} t) \quad (4)$$

we can re-express (1) and (2) as

$$v_{i(I)}(t) = (1+\varepsilon)\{\cos(\theta) v_{x(I)}(t) - \sin(\theta) v_{x(Q)}(t)\} \quad (5)$$

and

$$v_{i(Q)}(t) = (1-\varepsilon)\{\cos(\theta) v_{x(Q)}(t) - \sin(\theta) v_{x(I)}(t)\} \quad (6)$$

respectively.

Fig. 2 represents mismatch in quadrature mixing in accordance to (5) and (6).

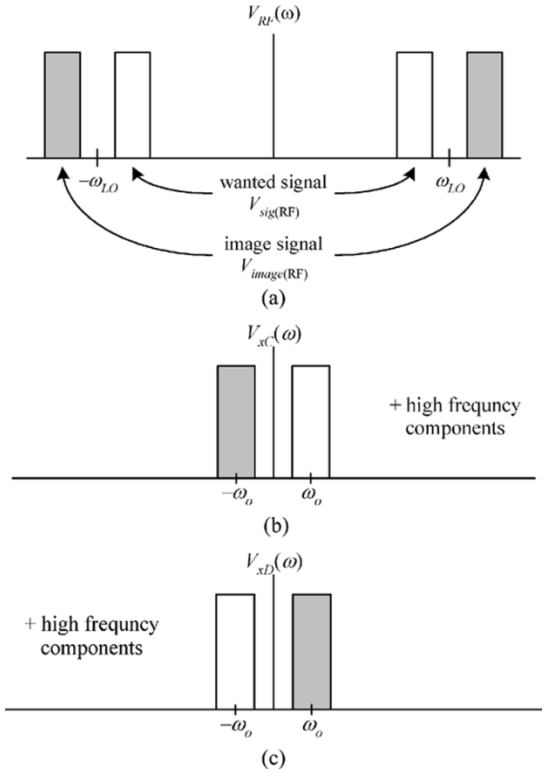

Fig. 3. Spectra of (a) $v_{\rm RF}$, (b) v_{xC}, and (c) v_{xD}.

We now define two complex signals

$$v_{xC}(t) = v_{x(I)}(t) + jv_{x(Q)}(t) \tag{7}$$

and

$$v_{xD}(t) = v_{x(I)}(t) - jv_{x(Q)}(t). \tag{8}$$

Fig. 3(a) shows spectral components of $v_{\rm RF}(t)$ where we ignore other channel signals. According to (3)–(4) and (7)–(8), by neglecting higher frequency components, it can be mathematically shown that

$$V_{xC}(\omega) = V_{\rm sig}(\omega - \omega_o) + V_{\rm image}(\omega + \omega_o) \tag{9}$$

and

$$V_{xD}(\omega) = V^*_{\rm sig}(-\omega - \omega_o) + V^*_{\rm image}(-\omega + \omega_o) \tag{10}$$

where $V_{\rm sig}(\omega)$ and $V_{\rm image}(\omega)$ are complex baseband signals of $V_{\rm sig(RF)}$ and $V_{\rm image(RF)}$, respectively

Fig. 3(b) and (c) shows graphical representation of (9) and (10), respectively, where it can be seen that $V_{xC}(\omega)$ and $V_{xD}(\omega)$ are mirror images of each other.

Referring to Fig. 2, by defining $V_{iC} = V_{i(I)} + jV_{i(Q)}$, $V_{iD} = V_{i(I)} - jV_{i(Q)}$ and $V_{oC} = V_{o(I)} + jV_{o(Q)}$, it can be generally shown that [5], [6]

$$V_{oC}(\omega) = H_S(\omega)V_{iC}(\omega) + H_M(\omega)V_{iD}(\omega). \tag{11}$$

According to (11), it can be seen that the complex output signal, V_{oC}, comprises the filtered version of both the complex signals V_{iC} and its mirror image V_{iD}. In a perfect matching case, $H_M(\omega)$ would be zero and there is no cross-contribution from V_{iD} to V_{oC}.

The derivation of $H_S(\omega)$ and $H_M(\omega)$ for complex G_m–C filter can be found in [5]. The expressions of $H_S(\omega)$ and $H_M(\omega)$ for complex G_m–C filter are as follows. Referring to Fig. 4, we define

$$\begin{aligned}
\boldsymbol{\omega}_{\mathbf{oz}} &= \frac{1}{2}(\boldsymbol{\omega}_{\mathbf{ox}} + \boldsymbol{\omega}_{\mathbf{oy}}) \\
\Delta\boldsymbol{\omega}_{\mathbf{o}} &= \frac{1}{2}(\boldsymbol{\omega}_{\mathbf{oy}} - \boldsymbol{\omega}_{\mathbf{ox}}) \\
\boldsymbol{\omega}_{\mathbf{uz}} &= \frac{1}{2}(\boldsymbol{\omega}_{\mathbf{ux}} + \boldsymbol{\omega}_{\mathbf{uy}}) \\
\Delta\boldsymbol{\omega}_{\mathbf{u}} &= \frac{1}{2}(\boldsymbol{\omega}_{\mathbf{uy}} - \boldsymbol{\omega}_{\mathbf{ux}}) \\
\boldsymbol{\omega}_{\mathbf{iz}} &= \frac{1}{2}(\boldsymbol{\omega}_{\mathbf{ix}} + \boldsymbol{\omega}_{\mathbf{iy}}) \\
\Delta\boldsymbol{\omega}_{\mathbf{i}} &= \frac{1}{2}(\boldsymbol{\omega}_{\mathbf{iy}} - \boldsymbol{\omega}_{\mathbf{ix}})
\end{aligned}$$

where for $m, n = 1, 2, \ldots, N$

$$\boldsymbol{\omega}_{\mathbf{ox}_m} = \frac{G_{ox_m}}{C_{x_m}} \quad \boldsymbol{\omega}_{\mathbf{ux}_{mn}} = \frac{G_{ux_{mn}}}{C_{x_m}} \quad \boldsymbol{\omega}_{\mathbf{ix}_m} = \frac{G_{ix_m}}{C_{x_m}}$$
$$\boldsymbol{\omega}_{\mathbf{oy}_m} = \frac{G_{oy_m}}{C_{y_m}} \quad \boldsymbol{\omega}_{\mathbf{uy}_{mn}} = \frac{G_{uy_{mn}}}{C_{y_m}} \quad \boldsymbol{\omega}_{\mathbf{iy}_m} = \frac{G_{iy_m}}{C_{y_m}}$$

For $V_{oC} = V_{o(I)_k} + jV_{o(Q)_k}$, we have

$$H_S(\omega) = H_{S_k}(\omega) \qquad \text{and} \qquad H_M(\omega) = H_{M_k}(\omega)$$

$$\begin{aligned}
\text{where } \mathbf{H_S}(\omega) = &\left[\mathbf{A}(\omega)\mathbf{A}^*(-\omega) - \mathbf{A}(\omega)\mathbf{C}\mathbf{A}^{-1}(\omega)\mathbf{C}^*\right]^{-1} \\
&\cdot \mathbf{A}(\omega)\left[\boldsymbol{\omega}_{\mathbf{iz}} - \mathbf{C}\mathbf{A}^{-1}(\omega)\Delta\boldsymbol{\omega}_{\mathbf{i}}\right] \\
\text{and } \mathbf{H_M}(\omega) = &\left[\mathbf{A}(\omega)\mathbf{A}^*(-\omega) - \mathbf{A}(\omega)\mathbf{C}\mathbf{A}^{-1}(\omega)\mathbf{C}^*\right]^{-1} \\
&\cdot \mathbf{A}(\omega)\left[\mathbf{C}\mathbf{A}^{-1}(\omega)\boldsymbol{\omega}_{\mathbf{iz}} - \Delta\boldsymbol{\omega}_{\mathbf{i}}\right]
\end{aligned}$$

in which

$$\mathbf{A}(\omega) = j(\omega\mathbf{I} + \boldsymbol{\omega}_{\mathbf{oz}}) - \boldsymbol{\omega}_{\mathbf{uz}} \quad \text{and} \quad \mathbf{C} = j\Delta\boldsymbol{\omega}_{\mathbf{o}} - \Delta\boldsymbol{\omega}_{\mathbf{u}}.$$

For the case of the opamp-*RC* complex filters, the expressions of $H_S(\omega)$ and $H_M(\omega)$ can be found in [6].

By substituting Fourier transforms of (5) and (6) into (11) and re-arranging the results, we have

$$V_{oC}(\omega) = H_{\rm ST}(\omega)V_{xC}(\omega) + H_{\rm MT}(\omega)V_{xD}(\omega) \tag{12}$$

where

$$H_{\rm ST}(\omega) = H_S(\omega)\{\cos\theta + j\varepsilon\sin\theta\} + H_M(\omega)\{\varepsilon\cos\theta + j\sin\theta\} \tag{13}$$

and

$$H_{\rm MT}(\omega) = H_S(\omega)\{\varepsilon\cos\theta - j\sin\theta\} + H_M(\omega)\{\cos\theta - j\varepsilon\sin\theta\}. \tag{14}$$

Fig. 5 shows a graphical representation of (13) and (14) where it can be seen that $H_{\rm ST}(\omega)$ is a complex response that blocks the unwanted side of V_{xC} from passing through and $H_{\rm MT}(\omega)$ is a response due to both mismatch in complex filter and I/Q imbalance in quadrature local oscillator that causes signal from the unwanted side to leak into the wanted side of the spectrum and vice versa.

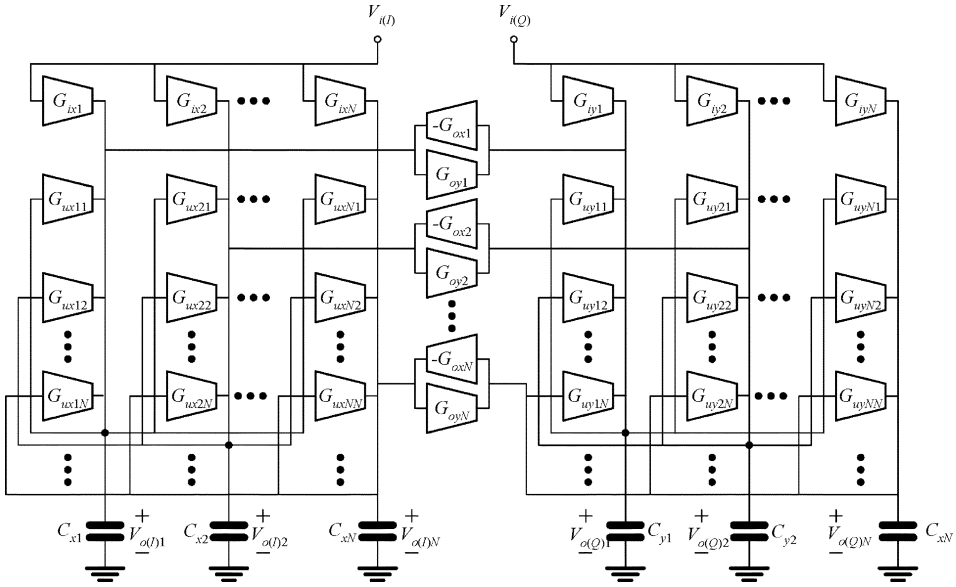

Fig. 4. General direct-state-space complex G_m–C filters.

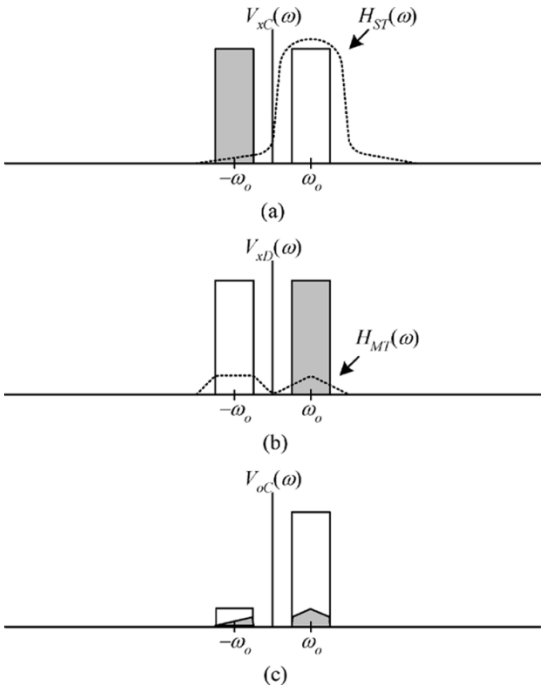

Fig. 5. Graphical representation of (13) and (14).

III. Signal-to–Interference Analysis

In this section, signal-to-interference ratio (SIR) at the end of the signal chain of the analog front end of the low-IF receivers will be analyzed. By substituting (9) and (10) into (12), we have

$$V_{oC}(\omega)=V_{\mathrm{sig}P}(\omega)+V_{\mathrm{image}P}(\omega)+V_{\mathrm{sig}N}(\omega)+V_{\mathrm{image}N}(\omega) \tag{15}$$

where

$$V_{\mathrm{sig}P}(\omega)=H_{\mathrm{ST}}(\omega)V_{\mathrm{sig}}(\omega-\omega_o) \tag{16}$$

and

$$V_{\mathrm{image}P}(\omega)=H_{\mathrm{MT}}(\omega)V^*_{\mathrm{image}}(-\omega+\omega_o) \tag{17}$$

are the wanted and image signals appeared in the positive side of Fig. 5(c), respectively, and

$$V_{\mathrm{sig}N}(\omega)=H_{\mathrm{MT}}(\omega)V^*_{\mathrm{sig}}(-\omega-\omega_o) \tag{18}$$

and

$$V_{\mathrm{image}N}(\omega)=H_{\mathrm{ST}}(\omega)V_{\mathrm{image}}(\omega+\omega_o) \tag{19}$$

are the wanted and image signals appeared in the negative side of Fig. 5(c), respectively.

It should be noted that unlike $V_{\mathrm{sig}N}(\omega)$ and $V_{\mathrm{image}N}(\omega)$, which are both out-of-band interference, $V_{\mathrm{image}P}(\omega)$ is the in-band inference, which cannot be removed by frequency-selective filtering.

According to (15)–(19), by defining $S_{\mathrm{sig}}(\omega)$ and $S_{\mathrm{image}}(\omega)$ as the power-spectral density of $V_{\mathrm{sig}}(\omega)$ and $V_{\mathrm{image}}(\omega)$, respectively, the SIR of the signal at the output of the complex filter is

$$\mathrm{SIR}=\frac{P_{\mathrm{sig}P}}{P_{\mathrm{image}P}+P_{\mathrm{sig}N}+P_{\mathrm{image}N}} \tag{20}$$

where

$$P_{\mathrm{sig}P}=\int_{\omega_o-\mathrm{BW}/2}^{\omega_o+\mathrm{BW}/2}S_{\mathrm{sig}}(\omega-\omega_o)\left|H_{\mathrm{ST}}(\omega)\right|^2d\omega \tag{21}$$

and

$$P_{\mathrm{image}P}=\int_{\omega_o-\mathrm{BW}/2}^{\omega_o+\mathrm{BW}/2}S_{\mathrm{image}}(-\omega+\omega_o)\left|H_{\mathrm{MT}}(\omega)\right|^2d\omega \tag{22}$$

are the normalized power of the wanted and image signals in the positive side of the spectrum, respectively, and

$$P_{\mathrm{sig}N}=\int_{-\omega_o-\mathrm{BW}/2}^{-\omega_o+\mathrm{BW}/2}S_{\mathrm{sig}}(-\omega-\omega_o)\left|H_{\mathrm{MT}}(\omega)\right|^2d\omega \tag{23}$$

and

$$P_{\mathrm{image}N}=\int_{-\omega_o-\mathrm{BW}/2}^{-\omega_o+\mathrm{BW}/2}S_{\mathrm{image}}(\omega+\omega_o)\left|H_{\mathrm{ST}}(\omega)\right|^2d\omega \tag{24}$$

are the normalized power of the wanted and image signals appeared in the negative side of the spectrum, respectively.

However, if we are interested only in the in-band interference, the signal to interference ratio in such a case is

$$\mathrm{SIR}_{\text{in-band}} = \frac{P_{\text{sig}P}}{P_{\text{image}P}}. \tag{25}$$

Also, in a special case where $H_S(\omega) = 1$ and $H_M(\omega) = 0$, i.e., when the complex filter is removed, we have

$$\begin{aligned} P_{\text{sig}P} &= \int_{\omega_o - \mathrm{BW}/2}^{\omega_o + \mathrm{BW}/2} S_{\text{sig}}(\omega - \omega_o)\left(\cos^2\theta + \varepsilon^2 \sin^2\theta\right) d\omega \\ &= \left(\cos^2\theta + \varepsilon^2 \sin^2\theta\right) P_{\text{sig}} \end{aligned} \tag{26}$$

and

$$\begin{aligned} P_{\text{image}P} &= \int_{\omega_o - \mathrm{BW}/2}^{\omega_o + \mathrm{BW}/2} S_{\text{image}}(-\omega + \omega_o)\left(\varepsilon^2 \cos^2\theta + \sin^2\theta\right) d\omega \\ &= \left(\varepsilon^2 \cos^2\theta + \sin^2\theta\right) P_{\text{image}} \end{aligned} \tag{27}$$

and thus

$$\mathrm{SIR}_{\text{in-band}} = \Phi\left(\frac{P_{\text{sig}}}{P_{\text{image}}}\right) \tag{28}$$

where

$$\begin{aligned} \Phi &= \frac{\cos^2\theta + \varepsilon^2 \sin^2\theta}{\varepsilon^2 \cos^2\theta + \sin^2\theta} \\ &= \frac{1 + \varepsilon^2 \tan^2\theta}{\varepsilon^2 + \tan^2\theta} \cong \frac{4}{\left(\frac{\Delta a}{a_o}\right)^2 + (\Delta\theta)^2} \end{aligned} \tag{29}$$

is equivalent to the quadrature attenuation L_{QUAD} in [4] and the image-rejection ratio (IRR) of the image-reject receiver [9]. For instance, for 0.5%-0.5° magnitude-phase imbalance in I/Q generation, the value of Φ is found to be approximately 44 dB.

According to the above analysis, the SIR cannot be computed without the knowledge of $S_{\text{sig}}(\omega)$ and $S_{\text{image}}(\omega)$. However, by using narrow-band approximation, i.e., assuming that $S_{\text{sig}}(\omega)$ and $S_{\text{image}}(\omega)$ are concentrated only near dc, according to (20) and (25), we found that

$$\mathrm{SIR}_{(NB)} = \frac{\left|H_{\mathrm{ST}}(\omega_o)\right|^2 P_{\text{sig}}}{\left|H_{\mathrm{MT}}(\omega_o)\right|^2 P_{\text{image}} + \left|H_{\mathrm{ST}}(-\omega_o)\right|^2 P_{\text{image}} + \left|H_{\mathrm{MT}}(-\omega_o)\right|^2 P_{\text{sig}}} \tag{30}$$

and

$$\mathrm{SIR}_{\text{in-band}(NB)} = \frac{\left|H_{\mathrm{ST}}(\omega_o)\right|^2 P_{\text{sig}}}{\left|H_{\mathrm{MT}}(\omega_o)\right|^2 P_{\text{image}}}. \tag{31}$$

Therefore, the values of $|H_{\mathrm{ST}}(\omega_o)|$, $|H_{\mathrm{MT}}(\omega_o)|$, $|H_{\mathrm{ST}}(-\omega_o)|$ and $|H_{\mathrm{MT}}(-\omega_o)|$ can be used as the performance indicators of the analog front-end section of the low-IF receiver.

IV. Simulation Results

Substituting $V_{xC} = V_{x(I)} + jV_{x(Q)}$, $V_{xD} = V_{x(I)} - jV_{x(Q)}$ and $V_{oC} = V_{o(I)} + jV_{o(Q)}$ into (12) yields

$$\begin{aligned} V_{o(I)}(\omega) + jV_{o(Q)}(\omega) = {} & H_{\mathrm{ST}}(\omega)\left\{V_{x(I)}(\omega) + jV_{x(Q)}(\omega)\right\} \\ & + H_{\mathrm{MT}}(\omega)\left\{V_{x(I)}(\omega) - jV_{x(Q)}(\omega)\right\}. \end{aligned} \tag{32}$$

According to the above equation, by letting $V_{x(I)} = 1$ an $V_{x(Q)} = -j$, we have

$$2H_{\mathrm{ST}}(\omega) = \left[V_{o(I)} + jV_{o(Q)}\right]_{V_{x(I)}=1, V_{x(Q)}=-j}. \tag{33}$$

By substituting $V_{o(I)} = \mathrm{Re}\{V_{o(I)}\} + j\mathrm{Im}\{V_{o(I)}\}$ and $V_{o(Q)} = \mathrm{Re}\{V_{o(Q)}\} + j\mathrm{Im}\{V_{o(Q)}\}$ into (33) and rearranging the result, we obtain

$$\begin{aligned} 2H_{\mathrm{ST}}(\omega) = {} & \left[\mathrm{Re}\left\{V_{o(I)}\right\} - \mathrm{Im}\left\{V_{o(Q)}\right\}\right]_{V_{x(I)}=1, V_{x(Q)}=-j} \\ & + j\left[\mathrm{Im}\left\{V_{o(I)}\right\} + \mathrm{Re}\left\{V_{o(Q)}\right\}\right]_{V_{x(I)}=1, V_{x(Q)}=-j}. \end{aligned} \tag{34}$$

Consequently, it can be shown that for

$$H_{Sx}(\omega) = \left[\mathrm{Re}\{V_{o(I)}\} - \mathrm{Im}\{V_{o(Q)}\}\right]_{V_{x(I)}=1, V_{x(Q)}=-j} \tag{35}$$

and

$$H_{Sy}(\omega) = \left[\mathrm{Im}\{V_{o(I)}\} + \mathrm{Re}\{V_{o(Q)}\}\right]_{V_{x(I)}=1, V_{x(Q)}=-j} \tag{36}$$

we have

$$H_{\mathrm{ST}}(\omega) = 0.5\left\{H_{Sx}(\omega) + jH_{Sy}(\omega)\right\}. \tag{37}$$

Now, it can be observed from Fig. 2 that applying

$$V_{x(I)} = 1 \qquad \text{and} \qquad V_{x(Q)} = -j$$

is equivalent to applying

$$V_{i(I)} = (1+\varepsilon)\exp(j\theta) \quad \text{and} \quad V_{i(Q)} = -j(1-\varepsilon)\exp(-j\theta)$$

to the input terminals of complex filter. As a result, the simulated magnitude and phase responses of $H_{\mathrm{ST}}(\omega)$ can be obtained from

$$\left|H_{\mathrm{ST}}(\omega)\right| = 0.5\sqrt{H_{\mathrm{ST}x}^2(\omega) + H_{\mathrm{ST}y}^2(\omega)} \tag{38}$$

and

$$\angle H_{\mathrm{ST}}(\omega) = \tan^{-1}\frac{H_{Sy}(\omega)}{H_{Sx}(\omega)} \tag{39}$$

respectively, where the equations at the bottom of the page are true.

Likewise, according to (32), by letting $V_{x(I)} = 1$ and $V_{x(Q)} = j$, we have

$$2H_{\mathrm{MT}}(\omega) = \left[V_{o(I)} + jV_{o(Q)}\right]_{V_{x(I)}=1, V_{x(Q)}=j}. \tag{40}$$

$$H_{Sx}(\omega) = \left[\mathrm{Re}\{V_{o(I)}\} - \mathrm{Im}\{V_{o(Q)}\}\right]_{V_{i(I)}=(1+\varepsilon)\exp(j\theta), V_{i(Q)}=-j(1-\varepsilon)\exp(-j\theta)}$$

$$H_{Sy}(\omega) = \left[\mathrm{Im}\{V_{o(I)}\} + \mathrm{Re}\{V_{o(Q)}\}\right]_{V_{i(I)}=(1+\varepsilon)\exp(j\theta), V_{i(Q)}=-j(1-\varepsilon)\exp(-j\theta)}$$

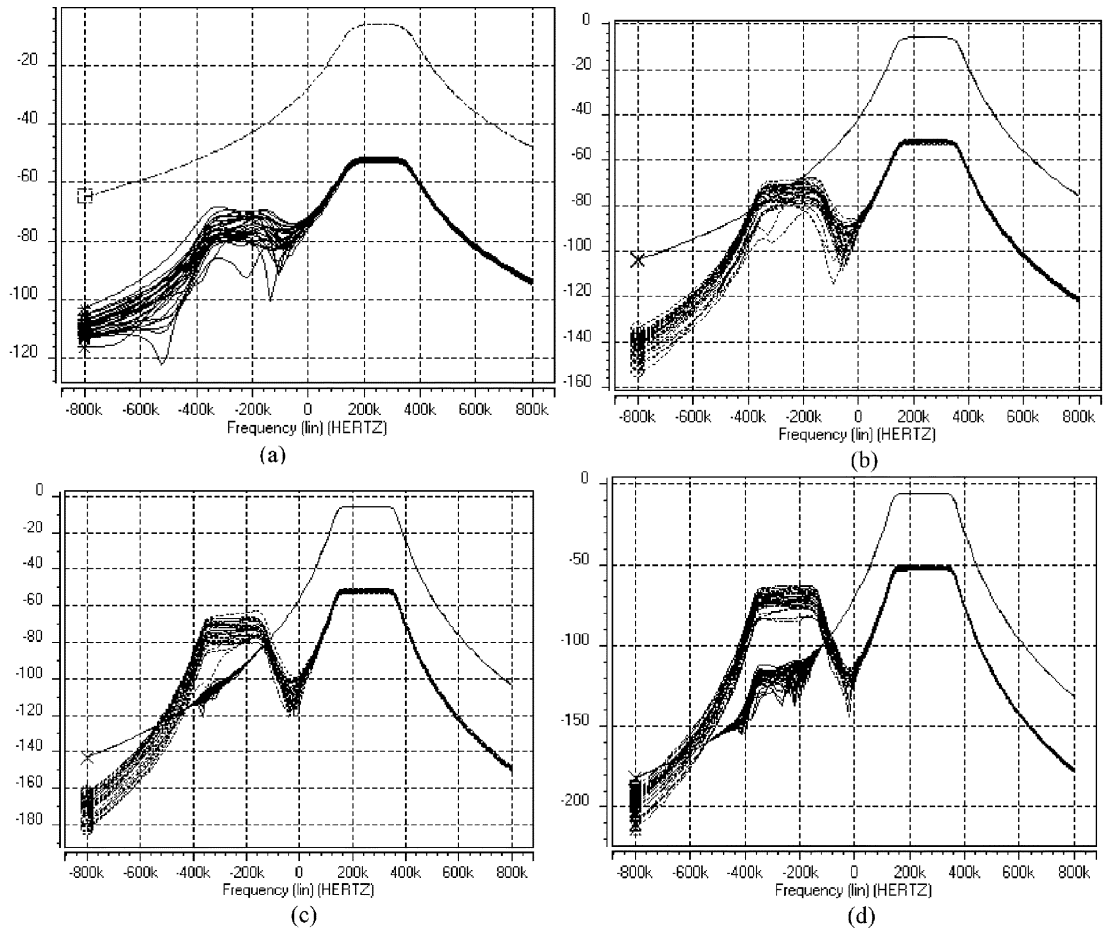

Fig. 6. Magnitude responses (in decibels) of $H_{\mathrm{ST}}(\omega)$ (upper curve) and $H_{\mathrm{MT}}(\omega)$ (lower curve) of the low-IF receivers employing G_m–C Butterworth filters of (a) third order, (b) fifth order, (c) seventh order, and (d) ninth order.

By substituting $V_{o(I)} = \mathrm{Re}\{V_{o(I)}\} + j\mathrm{Im}\{V_{o(I)}\}$ and $V_{o(Q)} = \mathrm{Re}\{V_{o(Q)}\} + j\mathrm{Im}\{V_{o(Q)}\}$ into (40) and rearranging the result, we obtain

$$2H_{\mathrm{MT}}(\omega) = \left[\mathrm{Re}\left\{V_{o(I)}\right\} - \mathrm{Im}\left\{V_{o(Q)}\right\}\right]_{V_{x(I)}=1, V_{x(Q)}=j} + j\left[\mathrm{Im}\left\{V_{o(I)}\right\} + \mathrm{Re}\left\{V_{o(Q)}\right\}\right]_{V_{x(I)}=1, V_{x(Q)}=j} \quad (41)$$

Consequently, it can be shown that for

$$H_{Mx}(\omega) = \left[\mathrm{Re}\{V_{o(I)}\} - \mathrm{Im}\{V_{o(Q)}\}\right]_{V_{x(I)}=1, V_{x(Q)}=j} \quad (42)$$

and

$$H_{My}(\omega) = \left[\mathrm{Im}\{V_{o(I)}\} + \mathrm{Re}\{V_{o(Q)}\}\right]_{V_{x(I)}=1, V_{x(Q)}=j} \quad (43)$$

we have

$$H_{\mathrm{MT}}(\omega) = 0.5\left\{H_{Mx}(\omega) + jH_{My}(\omega)\right\}. \quad (44)$$

Now, it can be observed from Fig. 2 that applying

$$V_{x(I)} = 1 \qquad \text{and} \qquad V_{x(Q)} = j$$

is equivalent to applying

$$V_{i(I)} = (1+\varepsilon)\exp(-j\theta) \quad \text{and} \quad V_{i(Q)} = j(1-\varepsilon)\exp(j\theta)$$

to the input terminals of complex filter. As a result, the simulated magnitude and phase responses of $H_{\mathrm{MT}}(\omega)$ can be obtained from

$$|H_{\mathrm{MT}}(\omega)| = 0.5\sqrt{H_{MTx}^2(\omega) + H_{MTy}^2(\omega)} \quad (45)$$

and

$$\angle H_{\mathrm{MT}}(\omega) = \tan^{-1}\frac{H_{My}(\omega)}{H_{Mx}(\omega)} \quad (46)$$

respectively, where the equations at the bottom of the page are true.

$$H_{Mx}(\omega) = \left[\mathrm{Re}\{V_{o(I)}\} - \mathrm{Im}\{V_{o(Q)}\}\right]_{V_{i(I)}=(1+\varepsilon)\exp(-j\theta), V_{i(Q)}=j(1-\varepsilon)\exp(j\theta)}$$
$$H_{My}(\omega) = \left[\mathrm{Im}\{V_{o(I)}\} + \mathrm{Re}\{V_{o(Q)}\}\right]_{V_{i(I)}=(1+\varepsilon)\exp(-j\theta), V_{i(Q)}=j(1-\varepsilon)\exp(j\theta)}$$

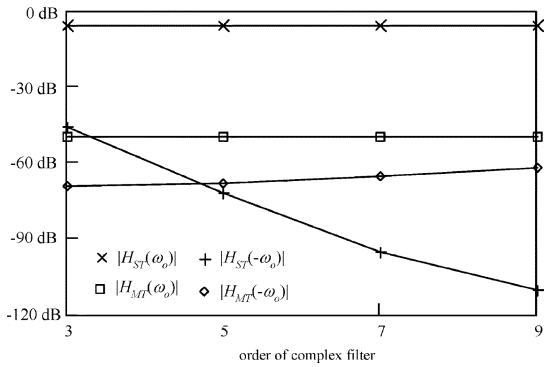

Fig. 7. Worst case simulated values of $|H_{\rm ST}(\omega_o)|, |H_{\rm MT}(\omega_o)|, |H_{\rm ST}(-\omega_o)|$ and $|H_{\rm MT}(-\omega_o)|$.

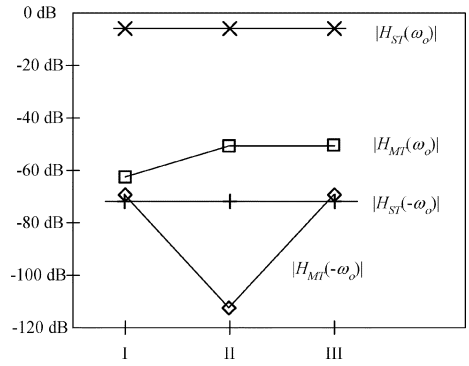

Fig. 8. Simulated performance parameters of the low-IF receiver employing fifth-order Butterworth complex filter with (I) only filter mismatch (II) only I/Q imbalance and (III) both I/Q imbalance and filter mismatch taken into account.

It should be pointed out here that although the voltages $v_{o(I)}(t)$ and $v_{o(Q)}(t)$ are real signals, the values of their spectral components, $V_{o(I)}(\omega)$ and $V_{o(Q)}(\omega)$, are in general complex. By performing ac analysis, the signals $V_{o(I)}(\omega)$ and $V_{o(Q)}(\omega)$ will be of complex values and so their real and imaginary parts (or alternatively, magnitude and phase) can be readily obtained from SPICE.

According to (38) and (45), for 0.5%-0.5° magnitude-phase imbalance in I/Q generation and 0.2% complex filter component mismatch, HSPICE Monte Carlo simulation results of the low-IF receivers employing G_m–C complex filters of various orders are shown in Fig. 6. The complex filters were derived from the doubly terminated Butterworth *LC*-ladder filter prototype and were designed to have a bandwidth of 220 kHz and a center frequency of 250 kHz.

The worst case values of the above simulation results are shown in Fig. 7. It can be seen that of the values of $|H_{\rm ST}(\omega_o)|$ and $|H_{\rm MT}(\omega_o)|$ change very little with the order of filter. Consequently, according to the narrow band approximation in (31), the $\rm SIR_{in\text{-}band}$ of the analog front-end of the low-IF receiver is largely independent on the order of filter.

On the other hand, the values of $|H_{\rm ST}(-\omega_o)|$ and $|H_{\rm MT}(-\omega_o)|$, which determine the level of the out-of-band interference, are dependent on the order of complex filter. As expected, the values of $|H_{\rm ST}(-\omega_o)|$ was found to decrease noticeably for the higher filter order. Unfortunately, the value of $|H_{\rm MT}(-\omega_o)|$ was found to be slightly increasing with the filter order and exceeding the value of $|H_{\rm ST}(-\omega_o)|$ when the filter order is 5. According to (30), this implies that, in certain situations, especially when $P_{\rm sig}$ is higher than $P_{\rm image}$, the level of out-of-band interference might increase with the order of filter.

By observing Fig. 8, it can be found that:

- the I/Q imbalance and complex filter mismatch hardly affect the values of both $|H_{\rm ST}(\omega_o)|$ and $|H_{\rm ST}(-\omega_o)|$;
- $|H_{\rm MT}(-\omega_o)|$ is dominated by the effect of complex filter mismatch;
- the effect of I/Q imbalance is the major contributor of $|H_{\rm MT}(\omega_o)|$.

The above observation implies that in this case, although the effect of complex filter mismatch on the in-band interference is only marginal, its effect on the out-of-band interference cannot be neglected. It should be noted that if the complex filter mismatch is not taken into consideration, the values of both $|H_{\rm ST}(\omega_o)|/|H_{\rm MT}(\omega_o)|$ and $|H_{\rm ST}(-\omega_o)|/|H_{\rm MT}(-\omega_o)|$ are about 44 dB, which is in agreement with (29).

V. Conclusion

Simulation results indicate that the SIR of the front-end of low-IF receiver is limited by the imbalance in quadrature down conversion and mismatch in complex filtering. Although the complex filter can ideally be used to suppress the out-of-band image interference by inhibiting the received image signal from passing through, it also causes the wanted signal to leak into the image channel and becomes part of the out-of-band interference.

Consequently, higher filter order does not necessarily result in the reduction of the out-of-band interference. In certain conditions, employing the polyphase filter of higher order might adversely increase the out-of-band interference, which in turn, deteriorates the signal to interference ratio. Therefore, in practice, the order of filter should not be selected based only on the ability to suppress the received image signal, as presented in [8]. The impact of mismatch, which inadvertently heightens the level of the out-of-band interference, has to be taken into consideration. In contrast, simulation results show that the in-band SIR is mainly independent of the order of the polyphase filter. This implies that the in-band SIR is mainly influenced by the imbalance during the I/Q downconversion, not the mismatch in complex filtering.

Acknowledgment

The author gratefully acknowledges the contributions of Mr. A. Boonmee to this work.

References

[1] J. Crol and M. S. J. Steyaert, "A single-chip 900 MHz CMOS receiver front-end with a high performace low-IF topology," *IEEE J. Solid-State Circuits*, vol. 30, no. 12, pp. 1483–1492, Dec. 1995.

[2] J. Crol and M. S. J. Steyaeart, "Low-IF topologies for high-performance analog front ends of fully integrated receivers," *IEEE Trans. Circuits Syst. II, Analog Digit. Signal Process.*, vol. 45, no. 3, pp. 269–282, Mar. 1998.

[3] B. Razavi, "Architecture and circuits for RF CMOS receivers," in *Proc. IEEE Custom Integrated Circuits Conf.*, Santa Clara, CA, May 1998, pp. 393–400.

[4] M. Valkama, M. Renfors, and M. Koivenen, "Advanced methods for I/Q imbalance compensation in a communication receiver," *IEEE Trans. Signal Process.*, vol. 49, no. 10, pp. 2335–2344, Oct. 2001.
[5] J. Mahattanakul, "The effects of mismatch in G_m–C polyphase filters," *IEEE Trans. Circuits Syst. II, Analog Digit. Signal Process.*, vol. 52, no. 7, pp. 410–414, Jul. 2005.
[6] E. Stikwoort, "Polyphase filter section with OPAMPs," *IEEE Trans. Circuits Syst. II, Analog Digit. Signal Process.*, vol. 50, no. 6, pp. 376–378, Jun. 2003.
[7] V. Vidojkovic, J. van der Tang, A. van Roermund, and A. Leeuverburgh, "Receiver planning for a 1.8 – 2.5 GHz multi-standard front-end," in *Proc. Eur. Conf. Circuit Theory Design*, 2003, pp. II189–192.
[8] V. Vidojkovic, J. van der Tang, and A. van Roermund, "Low-IF receiver planning for the DECT system," in *Proc. ProRISC Workshop Circuits, Systems Signal Processing*, 2001, pp. 700–705.
[9] B. Razavi, *RF Microelectronics*. Upper Saddle River, NJ: Prentice-Hall, 1998.

Jirayuth Mahattanakul (S'91–M'98) was born in Bangkok, Thailand, in 1968. He received the B.Eng. degree from King Mongkut's Institute of Technology Ladkrabang, Bangkok, Thailand, in 1990, the M.S. degree from Florida Institute of Technology, Melbourne, in 1992, and the Ph.D. degree from Imperial College London, London, UK, in 1998, all in electrical engineering.

From 1992 to 1994, he was with TelecomAsia (now TRUE Corporation), Bangkok, Thailand, in the Network Planning and Engineering Division. In 1994, he joined Mahanakorn University of Technology, Bangkok, Thailand where he is currently the Dean of Graduate School and an Associate Professor of Electronic Engineering.

Dr. Mahattanakul was a member of the Executive Committee and a President of the Young Engineer Chapter of the Engineering Institute of Thailand under H.M. the King's Patronage. He is on the Committee of the IEEE Circuits and Systems Chapter—Thailand Section.